THE JOURNAL OF PHYSICAL CHEMISTRY C
Article
pubs.acs.org/JPCC

Electrical and Photoelectrochemical Properties of WO_3/Si Tandem Photoelectrodes

Robert H. Coridan, Matthew Shaner, Craig Wiggenhorn, Bruce S. Brunschwig, and Nathan S. Lewis*

Kavli Nanoscience Institute, Beckman Institute and Joint Center for Artificial Photosynthesis, Division of Chemistry and Chemical Engineering, 210 Noyes Laboratory, 127-72, California Institute of Technology, Pasadena, California 91125, United States

S *Supporting Information*

ABSTRACT: Tungsten trioxide (WO_3) has been investigated as a photoanode for water oxidation reactions in acidic aqueous conditions. Though WO_3 is not capable of performing unassisted solar-driven water splitting, WO_3 can in principle be coupled with a low band gap semiconductor, such as Si, to produce a stand-alone, tandem photocathode/photoanode p-Si/n-WO_3 system for solar fuels production. Junctions between Si and WO_3, with and without intervening ohmic contacts, were therefore prepared and investigated in detail. Thin films of n-WO_3 that were prepared directly on p-Si and n-Si substrates exhibited an onset of photocurrent at a potential consistent with expectations based on the band-edge alignment of these two materials predicted by Andersen theory. However, n-WO_3 films deposited on Si substrates exhibited much lower anodic photocurrent densities (~0.02 mA cm^{-2} at 1.0 V vs SCE) than identically prepared n-WO_3 films that were deposited on fluorine-doped tin oxide (FTO) substrates (0.45 mA cm^{-2} at 1.0 V vs SCE). Deposition of n-WO_3 onto a thin layer of tin-doped indium oxide (ITO) that had been deposited on a Si substrate yielded anodic photocurrent densities that were comparable to those observed for n-WO_3 films that had been deposited onto FTO-coated glass. An increased photovoltage was observed when an n-Si/ITO Schottky junction was formed in series with the n-WO_3 film, relative to when the WO_3 was deposited directly onto the Si. Hence, inclusion of the ITO layer allowed for tandem photoelectrochemical devices to be prepared using n-WO_3 and n-Si as the light absorbers.

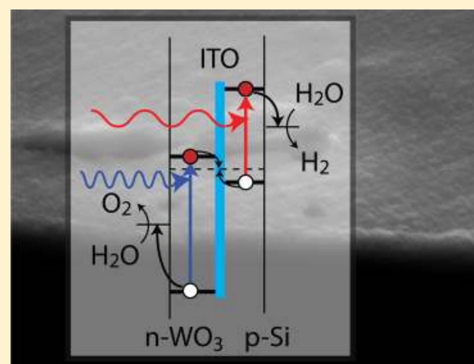

I. INTRODUCTION

Tandem photoelectrode systems are of interest for solar-driven water splitting. In one implementation of a tandem system, some of the photogenerated carriers are separated in a large band gap, n-type light absorber, with the resulting photogenerated holes driven by the electric field to the interface to perform oxidation reactions and the photogenerated electrons driven away from the semiconductor/liquid junction. A small band gap, p-type photocathode would then provide photogenerated electrons for the production of H_2(g), along with photogenerated holes that are driven into the bulk of the photocathode. The photogenerated holes would recombine with the photogenerated electrons at the interface between the anode and the cathode. This majority-carrier recombination maintains charge neutrality and allows for the interfacial electrochemical processes to occur continuously under steady-state illumination. The approach represents one embodiment of a "Z-scheme" design[1] (Figure 1a), designated as such by analogy to the energetics of the initial charge generation and separation steps in biological photosynthesis.

Silicon is a well-studied material that has been demonstrated to effect photocathodic H_2 production.[2] Additionally, Si is stable under photocathodic conditions in acidic solutions. However, Si does not have a sufficiently large band gap to produce the minimum photovoltage required thermodynamically to split water under standard conditions. Additionally, Si forms SiO_2 under anodic bias in aqueous solutions.[3] Strategies to couple Si photocathodes to a material that operates as a suitable photoanode are therefore of interest in the development of a tandem water-splitting device. Metal oxide overlayers have been used to enhance the photoactivity as well as to protect Si from oxidation under anodic operation.[4,5] Devices have also been prepared using a metal oxide thin film in tandem with amorphous Si or Si−Ge p−n junctions to perform the full water-splitting reaction without bias under solar illumination.[6]

Tungsten trioxide (WO_3) is an n-type metal oxide with a band gap (2.7 eV) that allows for absorption of visible light. WO_3 has a sufficiently positive potential of the top of its valence-band edge to oxidize water (E_{VB} ~ 3.1 V vs the normal hydrogen electrode, NHE), and like Si, WO_3 is stable in acidic aqueous solutions. The potential of the bottom of the conduction-band edge of WO_3 (E_{CB} ~ 0.3 V vs NHE) is nearly aligned with the potential of the top of the valence-band edge of Si (E_{VB} ~ 0.5 V vs NHE).[7,8] The interfacial energetics therefore allow, in principle, for majority carriers from n-WO_3

Received: December 5, 2012
Revised: February 22, 2013
Published: March 15, 2013

ACS Publications © 2013 American Chemical Society

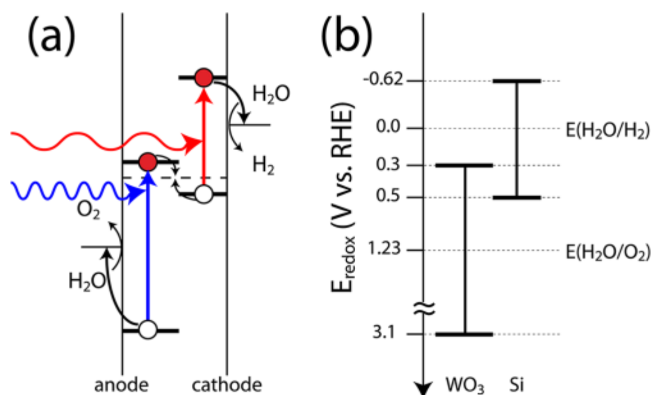

Figure 1. (a) Band energetics of a "Z-scheme" photoelectrochemical device for solar-driven water splitting. Illumination is incident on the n-type photoanode, where holes from the large band gap material oxidize water at the semiconductor/liquid interface. Photons that are transmitted through the photoanode can be absorbed in the smaller band gap photocathode. Photoexcited electrons in the cathode reduce water to H_2(g) at its semiconductor/liquid interface. The conduction band in the photoanode and the valence band in the photocathode are aligned so that the majority carriers from each material recombine at the metallurgical junction. (b) Band energetics of WO_3 and Si compared to the potentials for evolution of H_2 and O_2, respectively, from water.[7,8]

and p-Si to flow across the metallurgical interface without the need to overcome a large junction potential (Figure 1b).

The performance of a system based on this specific pair of absorbers depends not only on the properties of the individual components but also on the electrical properties of the interface between the Si and the WO_3. Specifically, carrier transport between the light absorbers must occur with a minimal barrier and with acceptable interfacial recombination velocities. In this work, the interfacial electrical properties of several types of Si/n-WO_3 structures have been investigated, with the goal of identifying approaches that can enable the use of this pair of materials as an anode/cathode tandem light absorber pair for solar-driven water splitting.

II. MATERIALS AND METHODS

Tungsten powder (Aldrich, >99.9% trace metals basis) and platinum black (Aldrich) were used as received. All water was 18 MΩ·cm in resistivity, as produced by a Barnstead Nanopure system. Buffered hydrofluoric acid (Transene, Inc.; referred to as BHF) was used as received. All other chemicals were ACS reagents or higher purity.

n-Type Si (Czochralski (CZ) grown, (100)-oriented, phosphorus-doped, 1−3 Ω·cm resistivity; n-Si), p-type Si (CZ-grown, (111)-oriented, B-doped, 4−12 Ω·cm; p-Si), or degenerately doped p-type Si (CZ-grown, (111)-oriented, B-doped, <0.001 Ω·cm; p^+-Si) wafers were used as substrates for the deposition of WO_3. Glass that had been coated with fluorine-doped tin oxide (Hartford Glass, TEC-15; FTO) was also used as a substrate for the deposition of WO_3. The indium−tin oxide (ITO) sputtering target (Plasmaterials, Inc., 99.99% pure) consisted of 90%:10% In_2O_3:SnO_2. Sputtered films were prepared using an RF magnetron sputtering system (AJA International).

A. Preparation of Substrates for Electrodeposition.

1. Fluorine-Doped Tin Oxide Substrates. Fluorine-doped tin oxide (FTO) coated glass substrates were sonicated sequentially in acetone, methanol, isopropanol, and water and were then dried with N_2(g). Electrodes were protected from making electrical contact to the solution by masking the entire surface area, except in the location where deposition was desired, with acrylic nail polish. Electrical contact to the FTO was made with an alligator clip while ensuring that the clip was not in contact with the electrolyte solution.

2. Si Substrates. Si substrates for electrodeposition were prepared by scratching Ga−In eutectic into the backside of the Si wafer. High-purity Ag paint (05002-AB, SPI Supplies) was then used to connect the sample to a Sn-coated Cu wire. The exposed electrode area was defined by using acrylic nail polish to mask the rest of the sample, including the electrical connection on the backside of the wafer, from the solution. These bare Si substrates were dipped in BHF for 30 s prior to electrodeposition to remove the native oxide layer from the Si surface.

3. ITO-Coated Si Substrates. To prepare Si for coating with ITO, bare Si samples were dipped in buffered HF(aq) (Transene, Inc.), BHF, for 30 s and then promptly (within 5 min) inserted into a sputtering chamber and pumped down to $<10^{-5}$ Torr. 100 nm of ITO was then sputtered onto the Si, with the sputtering occurring at room temperature in a 3 mTorr atmosphere of ultrahigh-purity Ar (20 sccm flow rate) and 95%/5% Ar/O_2 (0.75 sccm flow rate). The ITO was deposited at a rate of 1.15 nm min^{-1}, as measured by a quartz crystal thickness monitor.

For deposition of WO_3 films, electrical contact was made to the ITO layer by attaching an alligator clip to an area of the substrate that was physically not in contact with the electrodeposition bath. The electrodeposition area was defined by coating the rest of the submerged part of the substrate with acrylic nail polish, while leaving an area of ITO in contact with bath. Prior to electrodeposition, these substrates were rinsed with isopropanol and water, then dried in a stream of N_2(g).

B. Preparation of Tungsten Trioxide Photoanodes.

A peroxytungstic acid electroplating solution was prepared by gradually dissolving 4.6 g of tungsten powder in 50 mL of hydrogen peroxide (30% w/w). This solution was maintained in a constant temperature bath to prevent the exothermic reaction from boiling the solvent. After the powder had dissolved completely, a small amount of Pt black was added to the solution to decompose any remaining H_2O_2. When the H_2O_2 concentration was <3 mg L^{-1}, the solution was filtered to remove the Pt black and diluted to yield a final W concentration of 50 mM in 65%:35% H_2O:isopropanol.

Tungsten trioxide films were produced by galvanodynamic electrodeposition (Princeton Applied Research model 362 potentiostat), using a method that was similar to that described previously.[9,10] The electrodeposition current density was varied linearly, with a period of 6 s, between 0 and −0.4 mA cm^{-2}. After each electrodeposition, the nail polish masking layers were removed and the sample was annealed in air for 20 min at 275 °C. Cracking was observed in films that were prepared using deposition times that exceeded 40 min. Thick films were therefore deposited progressively by repeating the electrodeposition and annealing process for a total electrodepositon time of up to 60 min. WO_3 films on Si were prepared by use of two 15 min depositions because pronounced cracking occurred on these substrates when films were prepared using deposition times that exceeded 15 min. After the desired cumulative electrodeposition time had been reached, the samples were dried under a stream N_2(g), removed from their wires, and annealed in air for 2 h at 500 °C. To facilitate intercomparison

between the behaviors of WO_3 on the various types of substrates, the WO_3 films grown on Si-ITO, and on FTO, were prepared using two 15 or 30 min electrodeposition and annealing steps.

The samples prepared on Si, including Si/ITO samples, were then made into photoelectrodes. The large Si/ITO electrodeposition substrates were scored and diced into smaller samples. Electrical contact to these smaller samples was then made by scratching Ga–In eutectic into the back of the wafer. The sample was then mounted to a Sn-coated Cu wire with conductive Ag paint. After allowing the paint to dry, the wires were threaded through glass tubing and the edges of the substrate were sealed with epoxy (Hysol 1C, Loctite) and cured in air for at least 24 h. For samples prepared on FTO, the electrode area was defined with epoxy and the electrodes were allowed to cure for at least 24 h in air. A portion of the FTO sample was left uncovered by epoxy so that electrical contact could be made to the FTO by use of an alligator clip that was positioned physically out of contact with the solution. The functional area of all electrodes was measured by use of a 600 dpi scanner in conjunction with ImageJ image processing software.

C. Current–Voltage Measurements of Buried Si/ITO Junctions with a Dual-Contact Electrode. To investigate simultaneously the electrical properties of Si/ITO and ITO/n-WO_3 junctions, a 900 nm thick WO_3 film was prepared by use of three sequential 30 min electrodeposition processes on an n-Si/ITO substrate. After annealing, most of the sample was sealed in epoxy, and only the WO_3 thin film that defined the photoelectrode, as well as small areas that were used to produce contacts to the ITO and Si, respectively, were exposed. The Si was scratched with Ga–In to make an ohmic contact. Steel alligator clips were used to make electrical contact to the Si/Ga–In contact and to the ITO, respectively, as a dual-contact electrode. When used as an electrode, these small exposed contacting areas were not in contact with the electrolyte.

D. Photoelectrochemical Experiments. Cyclic voltammograms were measured in a standard three-compartment, glass electrochemical cell that was equipped with a standard calomel (SCE) reference electrode (CH Instruments), a Pt wire counter electrode, and 1.0 M HCl(aq) as the electrolyte. A quartz window was epoxied in front of the working electrode compartment to allow the sample to be illuminated by visible and near-ultraviolet light. The light source was a 150 W Xe arc lamp (Oriel), mounted with a collimator. Light was passed through an Air Mass (AM)1.5 filter prior to being incident on the photoelectrodes. The illumination intensity was set to produce, at the position of the sample, the same current density on a calibrated Si photodiode (FDS1010, Thorlabs) that was produced by 100 mW cm^{-2} of AM1.5G sunlight. All photoelectrochemical data were collected using a BAS 100B potentiostat (Bioanalytical Systems, Inc.).

E. Structural Characterization. X-ray diffraction patterns (XRD) were obtained using a PANalytical X'Pert PRO diffractometer with Cu Kα radiation. Scanning-electron micrograph (SEM) images were taken with a Zeiss model 1550VP SEM. Film thicknesses were measured with a DekTak model 3030 profilometer.

X-ray photoelectron spectroscopy (XPS) measurements were performed on an M-Probe instrument that was interfaced to ESCA HAWK control software (Service Physics, Inc.). Incident X-rays (Al Kα, 1486.6 eV) were directed at 35° from the sample plane. Ejected photoelectrons were collected by a hemispherical analyzer that was oriented at 35° from the sample plane. The reported spectra were collected in high-resolution mode ($\delta E \approx 0.8$ eV). Ar-plasma sputter depth profiling measurements were conducted at a base pressure of 10^{-7} Torr.

III. RESULTS

A. Characterization of WO_3 Films. Before annealing, electrodeposited WO_3 films were soft, gel-like, and susceptible to damage by solvents such as acetone as well as by drying under a stream of N_2(g). Electrodeposition of WO_3 on FTO-coated glass produced a dark blue film, whereas after the annealing step, the film was transparent and green-yellow. WO_3 films deposited on Si and Si-ITO samples appeared to change color as a function of their thickness due to thin film interference effects.

SEM images indicated that the electrodeposited WO_3 films were comprised of grains with diameters of 50–200 nm (Figure 2 and Figure SI.1). Micron-scale cracks were observed in films that were grown in a single step, possibly due to shrinking of the films during annealing. Multiple electrodeposition/anneal cycles filled in these cracks, and produced thicker and more uniform films. The annealed WO_3 films were monoclinic, as indicated by X-ray diffraction data (Figure 3). Profilometry measurements of galvanodynamically deposited WO_3 films indicated that the deposition rate was linearly proportional to the peak cathodic deposition current density, with a deposition rate of 10 nm min^{-1} observed for a peak current density of −0.4 mA cm^{-2}. These results are consistent with prior measurements of the relationship between the number of W atoms deposited and the total charge passed during deposition.[9]

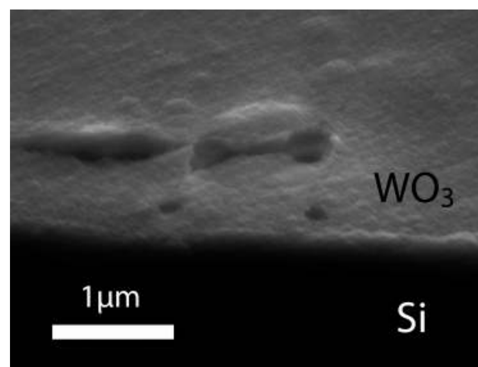

Figure 2. Cross section of an electrodeposited WO_3 thin film (white) on a Si substrate (black). The film is roughly 300 nm thick.

B. Photoelectrochemistry of WO_3 Films on Si. Figure 4a displays the cyclic voltammetric current density vs potential (J–E) behavior in 1.0 M HCl of a 300 nm thick WO_3 film on FTO-coated glass. At potentials close to 0 V vs SCE, peaks characteristic of the reduction and oxidation of WO_3 were observed in both the presence and absence of illumination.[11] Under illumination, the onset of photocurrent occurred at +0.35 V vs SCE, with a light-limited photocurrent density of 0.45 mA cm^{-2} at E = 1.0 V vs SCE for this film thickness.[12] Increases in the film thickness produced an increase in the photocurrent density,[10,13] consistent with the larger than 300 nm absorption length for most photons having an energy above the band gap energy of WO_3.[12] In acidic conditions, without the addition of an O_2-evolution catalyst, WO_3 has been shown

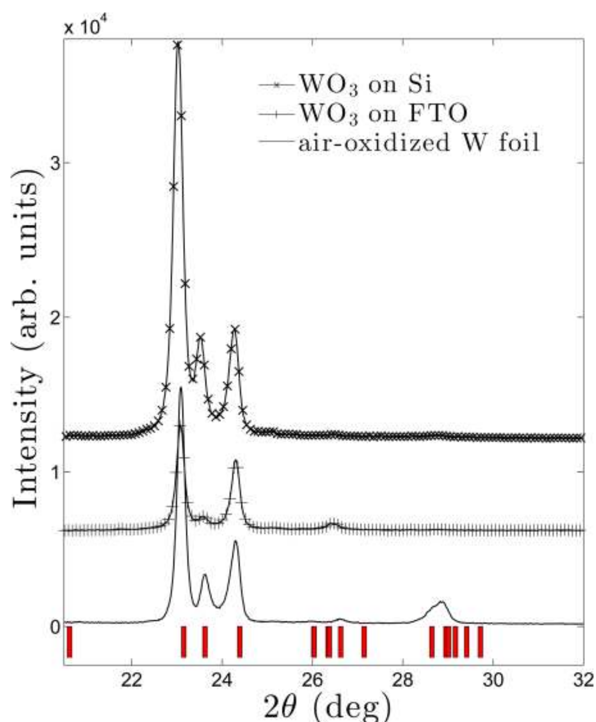

Figure 3. Powder XRD measurements from (−) a W foil oxidized in air to produce WO_3; electrodeposited and annealed WO_3 on (+) FTO-coated glass and (×) on p-Si(111). Each XRD pattern was corrected for shifts in the measured peak positions due to the finite thicknesses of the deposition substrates. The red ticks below the data indicate the peak positions for the known crystal structure of monoclinic tungsten trioxide at room temperature.[23] The intense features at $2\theta = 23.1°$. 23.6°, and 24.4° represent the ⟨002⟩, ⟨020⟩, and ⟨200⟩ Bragg reflections, respectively, for this phase.

to preferentially oxidize acid anions rather than oxidize water.[10] Because O_2 is not the product of photooxidation, no significant change was observed in the $J-E$ data of WO_3 electrodes in 1.0 M HCl when the electrolyte was deoxygenated by bubbling Ar versus when the electrolyte was saturated by bubbling $O_2(g)$.

Figure 4b depicts the cyclic voltammetry in 1.0 M HCl of 300 nm thick WO_3 films on n-Si and p-Si substrates, rspectively. The onset potential for photocurrent in $J-E$ measurements of WO_3 on p-Si was comparable to that of WO_3 on FTO (Figure 4a), but the photocurrent density ($J_{max} = 0.017$ mA cm^{-2} at $E = 1$ V vs SCE) was significantly smaller for WO_3 on p-Si substrates than for WO_3 on FTO-coated glass substrates. Films of WO_3 on n-Si substrates also showed lower light-limited photocurrent densities than WO_3 films on FTO, but the onset potential was ∼0.2 V more negative for WO_3 film on n-Si than for FTO/n-WO_3 or p-Si/n-WO_3 samples (Figure 4).

The photocathodic performance of p-Si/n-WO_3 electrodes was also evaluated. Figure 5a shows the cyclic voltammetry in 1.0 M HCl of a p-Si/n-WO_3 electrode compared to identical measurements using a p-Si electrode. When cathodic current was passed (at negative potentials), the p-Si/n-WO_3 samples exhibited lower limiting photocurrent densities than p-Si, but the difference in photocurrent density was not as significant as was observed between the Si/n-WO_3 and FTO/n-WO_3 samples under anodic conditions (Figure 4). The p-Si/n-WO_3 samples exhibited an onset of cathodic current at more positive potentials than the uncoated p-Si cathodes, consistent with observations that WO_3 reduces the overpotential for the production of H_2 on p-Si.[14]

To assess the composition of the Si/n-WO_3 interface after electrodeposition of WO_3, thin layers of WO_3 were removed progressively by an Ar sputter gun, with XPS data collected on the surface that was exposed after each sputtering step. The

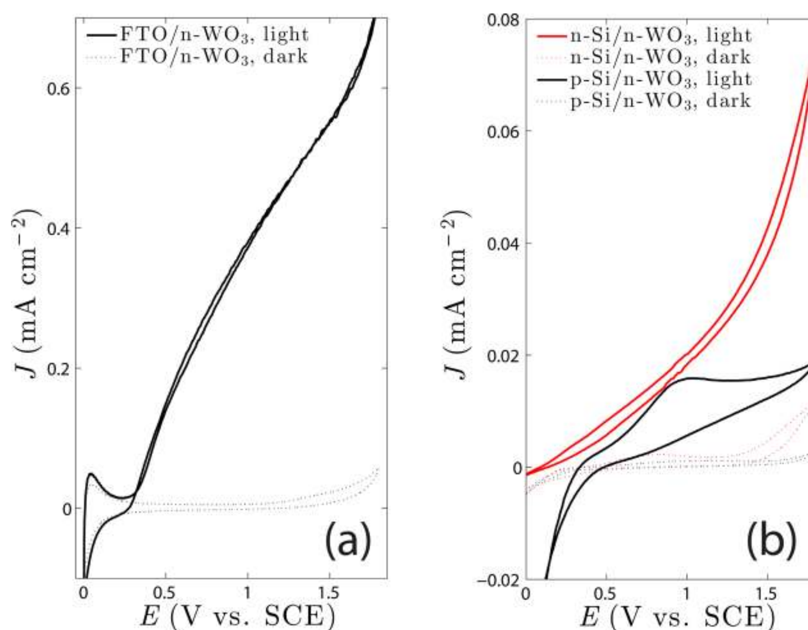

Figure 4. Cyclic voltammetry in 1.0 M HCl(aq) of WO_3 electrodeposited on (a) FTO-coated glass, (b) p-Si (black), and n-Si (red). The onset potential for photocurrent for the p-Si/n-WO_3 photoelectrode was similar to that for WO_3 on FTO, but the onset potential was shifted negatively for the n-Si/n-WO_3 photoelectrode, due to additional photovoltage generated at the n-Si/n-WO_3 heterojunction. The photocurrent densities for both Si/n-WO_3 electrodes were significantly lower than the photocurrent densities observed for WO_3 deposited onto FTO-coated glass (0.017 mA cm^{-2} for p-Si/n-WO_3 and 0.020 mA cm^{-2} n-Si/n-WO_3 versus 0.45 mA cm^{-2} for FTO/n-WO_3 at an electrode potential of +1.0 V vs SCE).

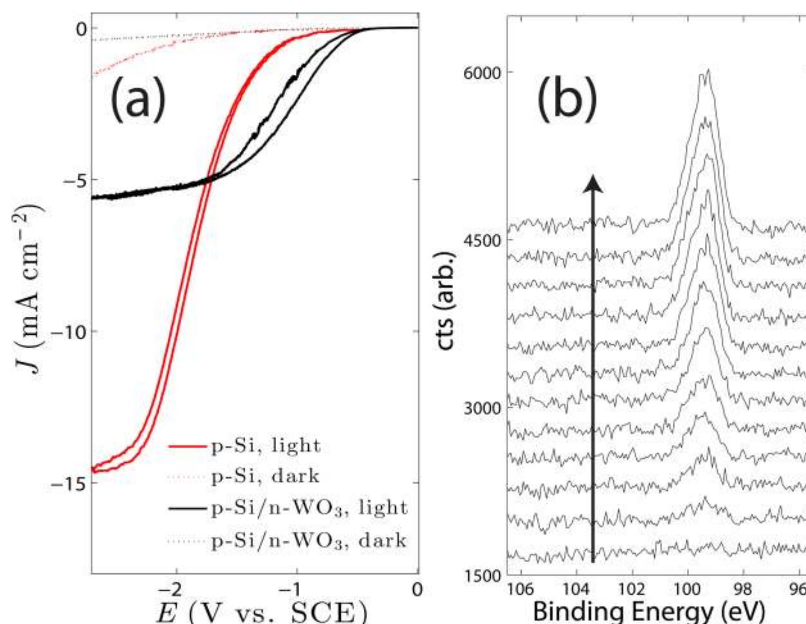

Figure 5. (a) Cyclic voltammetry in 1.0 M HCl(aq) of p-Si (red) and p-Si/n-WO_3 (black) electrodes. The addition of a WO_3 layer reduced the overall photocurrent by a factor of ∼2, but the onset potential for hydrogen evolution was shifted to more positive potentials (reduced overpotential) due to the increased catalytic activity of WO_3 relative to that of Si for evolution of H_2 from H_2O.[14] (b) Waterfall plot of depth profiling spectra of the Si 2p XPS peak of an n-Si electrode coated with a thin film of electrodeposited WO_3. This Si 2p peak was not detectable in the first scan (bottom). Each spectrum was measured sequentially after an 8 s Ar-ion sputter step, with the depth increasing in the direction of the arrow. The XPS spectra were dominated by the Si−Si feature at 99.5 eV, with no indication of the Si−O bonding feature at 103 eV that would be expected if an insulating silicon oxide layer had formed at the interface during deposition or annealing.

depth profile data in the Si 2p region of n-Si/n-WO_3 samples (Figure 5b) showed only the Si−Si bond feature, at a binding energy of 99.5 eV. No interfacial Si−O oxide (binding energy = 103 eV), which would have formed an insulating tunnel barrier between the WO_3 and the Si, was detectable by XPS.

C. Electrical Properties of ITO Films on Si. Figure 6a presents the current−voltage behavior of thin ITO films that had been deposited on Si surfaces that had been freshly etched with HF(aq). The p-Si/ITO junction was ohmic, whereas the n-Si/ITO junction was rectifying. This behavior is consistent with previous studies of ITO sputtered on Si.[15] XRD (Figure SI3.a) and SEM measurements (Figure SI3.b) indicated no detectable change between the structure of WO_3 films that had been deposited on these substrates relative to WO_3 films that had been deposited on FTO or on bare Si.

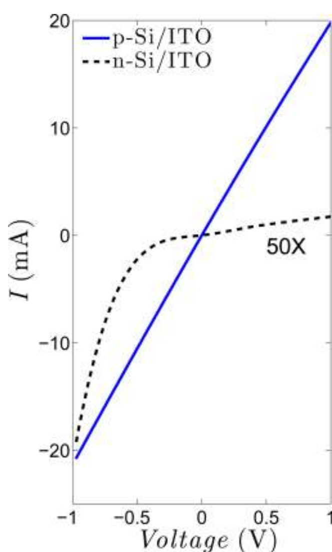

Figure 6. Electrical current−voltage behavior of p-Si/ITO (solid blue line, ohmic) and n-Si/ITO (dotted black line, rectifying, scaled by 50× to facilitate display on the same scale) junctions.

D. Photoelectrochemistry on WO_3/ITO/Si Layered Films. Figure 7a compares the J−E behavior of electrodeposited WO_3 films on p-Si/ITO substrates to the J−E behavior of WO_3 films on FTO substrates. When ITO was present, and provided an ohmic contact between the WO_3 and the Si, the observed photocurrent densities were comparable to, or larger than, those observed for FTO/n-WO_3 contacts. The onset potential for photocurrent was approximately the same for WO_3 on p-Si/ITO as for WO_3 on FTO (0.38 V vs SCE). On p-Si/ITO substrates, the photocurrent density increased when thicker WO_3 films, prepared by multistep electrodeposition, were used (Figure 7b).

Figure 7c depicts the effect of the Si doping on the photoresponse of Si/ITO/n-WO_3 electrodes. The Si/ITO/n-WO_3 contacts exhibited photocurrent densities that were comparable to those observed for FTO/n-WO_3 contacts. The p-Si/n-WO_3 and p^+-Si/n-WO_3 systems exhibited similar onset potentials for photoanodic current to that observed for FTO/n-WO_3 samples, consistent with the observation that p-Si and p^+-Si both made ohmic contact to ITO. The onset potential for WO_3 films on n-Si/ITO was shifted to more negative potentials than for Si/n-WO_3 contacts, indicating that the ITO intervening layer produced an additional photovoltage in the system, due to the n-Si/ITO Schottky barrier.

Figure 8 compares the voltammetric behavior observed when the n-Si, and separately when the ITO, were contacted in a n-Si/ITO/n-WO_3 dual-contact electrode system. The −0.18 V shift in onset potentials that was observed between the behavior

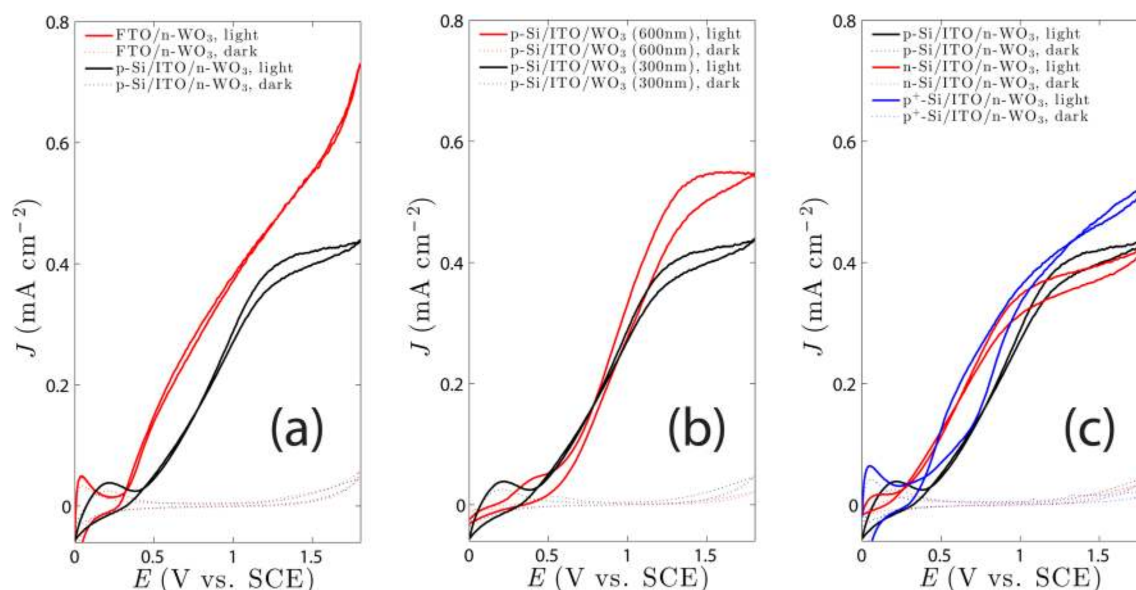

Figure 7. (a) Cyclic voltammetry in 1.0 M HCl(aq) of a 300 nm thick WO_3 film on a p-Si/ITO substrate (black). The 100 nm ITO layer formed an ohmic contact to both Si and WO_3, providing photocurrents comparable to those observed for films of WO_3 on FTO (red). (b) The photocurrent increased as the thickness of the WO_3 layer increased from 300 nm (black) to 600 nm (red). (c) Mutually similar photovoltages were observed for WO_3 prepared on p-Si/ITO (black) and p^+-Si/ITO (blue) due to the ohmic contact between the ITO layer and Si. The onset potential for photocurrent for WO_3 prepared on n-Si/ITO was shifted to negative potentials due to the buried n-Si/ITO Schottky junction.

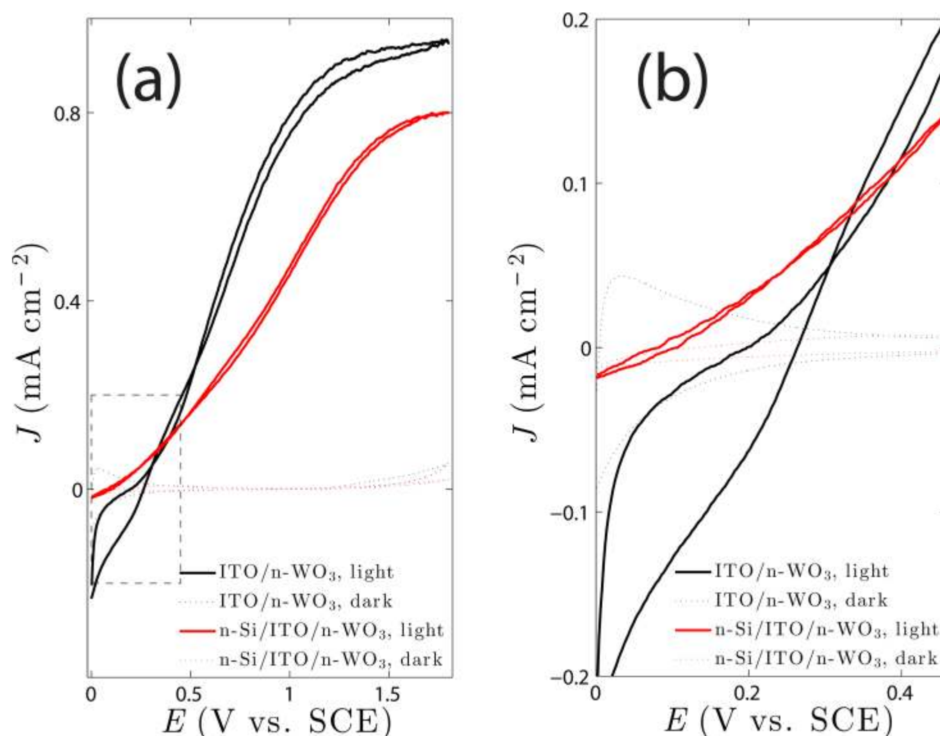

Figure 8. (a) Cyclic voltammetry in 1.0 M HCl(aq) of a 900 nm thick WO_3 film on an n-Si/ITO substrate. Electrical contact was made to both the ITO layer (effectively a ITO/n-WO_3 electrode, black) and to the n-Si (n-Si/ITO/n-WO_3 electrode, red) on the same sample. (b) A magnified view of the dashed box from (a). The onset potential for photocurrent of the n-Si/ITO/n-WO_3 CV shifted by ∼−180 mV relative to the behavior of ITO/n-WO_3 due to the additional photovoltage generated by the Schottky junction at the n-Si/ITO interface.

when the ITO was contacted, relative to when the Si was contacted, served as a measure of the photovoltage that was produced by the n-Si/ITO Schottky barrier in this sample. A similar shift in the onset potential for an n-Si/ITO/n-WO_3 electrode was observed in the J–E data of electrodes under red illumination (>580 nm), which can only generate carriers in Si (Figure SI.2). This shift is therefore due to the photovoltage generated at the n-Si/ITO Schottky junction. In contrast, no shift in the onset potential was observed for a p-Si/ITO/n-WO_3 photoelectrode under illumination with red light.

IV. DISCUSSION

The operation of a tandem structure depends not only on the band gaps of the materials but also on the band-edge alignment, as well as the electrical behavior of the junction between the absorbers of interest. Although the band-edge discontinuity can be predicted by Andersen theory,[16] many heterojunctions exhibit deviations from the theoretically expected behavior due to the presence of interfacial reactions when the heterojunction is formed and/or processed.[17] In principle, the p-Si/n-WO_3 system should have a band-edge alignment as depicted in Figure 1. This implies that an ohmic contact should be produced between p-Si and n-WO_3 and consequently that tandem behavior would be obtained by introduction of rectifying contacts to the n-WO_3 and p-Si surfaces, respectively. In addition, the band-edge alignment of Figure 1 predicts that a rectifying contact should be produced between n-Si and n-WO_3.

The behavior observed when WO_3 was electrodeposited directly onto Si is consistent with these predictions, although the limiting photocurrent densities were reduced significantly compared to those on the conductive FTO substrates. The potential at which the photocurrent exhibited an onset for the p-Si/n-WO_3 electrode was comparable to that for n-WO_3 on FTO, indicating that the interface acted essentially as an ohmic contact between the n-WO_3 and p-Si light absorbers in this structure. The peak in the p-Si/n-WO_3 data observed under illumination is coincident with the potentials required for the anodic oxidation of p-Si in acid. Cracks in the WO_3 film can expose small areas of the p-Si substrate to the electrolyte, with the consequent oxidation of the Si therefore a likely cause of the nonreversible J−E data in Figure 4b. For the n-Si/n-WO_3 electrode, the onset potential for photocurrent was shifted by −0.175 V compared to that observed for WO_3 films deposited onto FTO. In both Si doping cases, the photocurrent was significantly reduced (0.017 mA cm^{-2} at 1.0 V vs SCE for p-Si/n-WO_3, 0.020 mA cm^{-2} at 1.0 V vs SCE for n-Si/n-WO_3) compared to that for the n-WO_3 on FTO electrodes (0.45 mA cm^{-2} at 1.0 V vs SCE).

Although electrodeposition and high-temperature air annealing of the samples can lead to the formation of an insulating SiO_2 layer on Si, Si−O bonds were not observed at the Si/WO_3 interface in XPS sputter depth profiling measurements. The cathodic photocurrent through the interface was not reduced to the same extent as the photoanodic current, contrary to expectations for the presence of an insulating oxide at the interface. Strain due to lattice mismatch at the Si/WO_3 interface could also affect the transport of majority carriers, though recent theoretical calculations suggest only a slight lattice mismatch between the two materials.[18] Time-resolved photoluminescence studies of the interfacial recombination velocity of this system could elucidate the reason for the lower photocurrents observed for p-Si relative to the n-Si systems with WO_3 described herein.

Although the system studied herein produced low photocurrents, the shift in the onset potential of the n-Si/n-WO_3 structures relative to FTO/n-WO_3 systems suggests an interesting configuration for use in a tandem device structure. The potential of the Fermi level of n-Si is more negative than the potential of the bottom of the conduction-band edge of WO_3 (Figure 1), so when these materials equilibrate, electrons leave the n-Si and accumulate in the WO_3. The n-Si/n-WO_3 junction thus acts as a type II heterojunction that can provide a photovoltage in addition to the photovoltage generated at the WO_3 semiconductor/liquid junction. This behavior produces a negative shift in the potential for the onset of photocurrent for WO_3 deposited on n-Si relative to WO_3 itself, in accord with the experimental observations. The n-Si/n-WO_3 junction therefore acts in tandem with the n-WO_3-electrolyte junction and can utilize the photons of energy below the WO_3 band gap to provide this additional photovoltage in the system.

The p-Si/n-WO_3 electrode exhibited little change in photocurrent compared to the behavior of a H-terminated p-Si electrode operated under the same photocathodic conditions (Figure 5a). Further, no insulating oxide layer was observed at the interface in depth profiling experiments (Figure 5b). Hence, the reduction in current is not due to interfacial oxide formation during electrodeposition but is likely to be inherent to the transport properties of the Si/n-WO_3 interface.

Introduction of an intervening ITO layer yielded a significant increase in photocurrent relative to the photocurrent observed for the Si/n-WO_3/electrolyte structure. For all doping types of Si that were investigated, the anodic photocurrent density produced by the Si/ITO/n-WO_3 electrodes was comparable to the anodic current densities observed for the FTO/n-WO_3 electrodes. The potential for onset of photocurrent density for the p-Si/ITO/n-WO_3 electrode was similar to that for FTO/n-WO_3, which suggests that these materials could form the basis for a device similar to the one shown in Figure 1. The rectification observed for the n-Si/ITO junction implies that rather than using a semiconductor/liquid junction at the back and front side of a Z-scheme-based p-Si/n-WO_3 photoelectrochemical device, the tandem photovoltages in the n-Si/ITO/n-WO_3/electrolyte system can be obtained by use of a n-WO_3/electrolyte junction acting in concert with an n-Si/ITO Schottky barrier (Figure 9). An ohmic, catalytic back contact to the n-Si could then be formed, accompanied by deposition of Pt or other electrocatalysts, to produce H_2 with the majority-carrier electrons available at the back contact to the n-Si. This geometry is similar to monolithic tandem device designs that have been proposed previously.[19−21]

Although this system is convenient for studying the electrical contact properties of a Si/WO_3-based water-splitting device, the configuration described herein is not optimal for this application. The WO_3 films are too thin to collect all of the incident illumination above the band gap. This thickness should be chosen to maximize absorption in the photoanode and thereby maximize the overall efficiency of the device. Similarly, catalysts need to be incorporated into the design to perform the full water-splitting reaction rather than generate oxidized anions as the chemical products. When prepared in thin layers, ITO is the least resistive of the transparent conducting oxides,[22] but an In-based layer is inappropriate for large-scale technologies that aim to be based on earth-abundant materials. While ITO is useful for prototyping Si/n-WO_3 water-splitting devices or to easily couple new metal oxide materials to Si, other materials or deposition strategies should be investigated for this contacting layer. The electrode scheme described here can be further used to study the optimal light absorber thickness, structuring of semiconductors, and catalyst loading for the preparation of efficient materials for water-splitting applications.

For planar electrodes, an arrangement in which the components that generate the photovoltage are physically near the illuminated side of the device is appropriate. For the n-Si/ITO/n-WO_3 electrodes, all of the illumination below the n-WO_3 band gap is transmitted through the n-WO_3, permitting

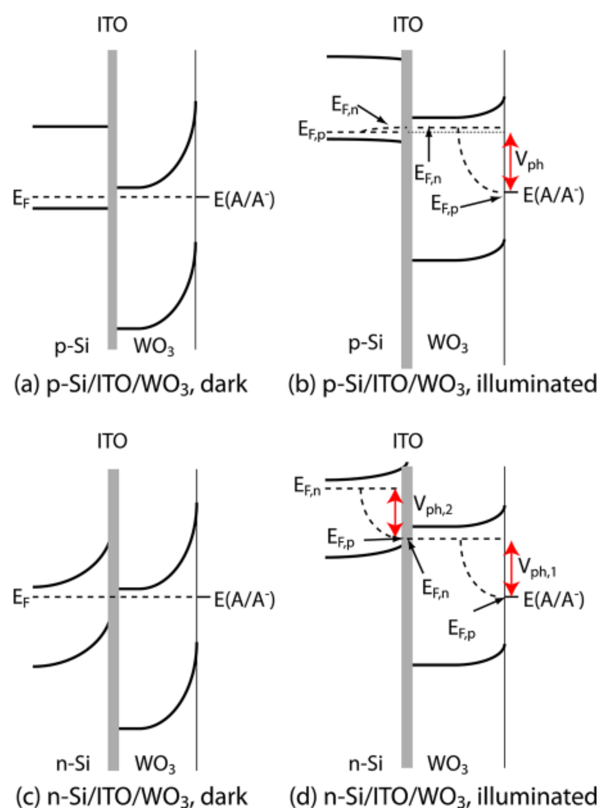

Figure 9. Band diagrams for p-Si/n-WO_3 and n-Si/n-WO_3 electrodes at equilibrium and under illumination, respectively. (a) For p-Si/n-WO_3 at equilibrium with a redox couple having a redox potential E(A/A$^-$), the band bending only occurs in the WO_3 layer. The band diagram for the p-Si/ITO/n-WO_3 case is identical because the ITO makes ohmic contact to both WO_3 and p-Si. (b) Under illumination, the quasi-Fermi levels of the holes ($E_{f,p}$) and of the electrons ($E_{f,n}$) split, generating a photovoltage in the WO_3 (V_{ph}). In the p-Si, majority carrier holes generated by light absorption recombine with electrons from the WO_3, resulting in a small split of the quasi-Fermi levels of electrons and holes in the p-Si. (c) In addition to the semiconductor–liquid junction, Fermi level equilibration across the n-Si/n-WO_3 interface generates an additional photoactive barrier because electrons leave the n-Si to accumulate in the WO_3. In contrast, in the n-Si/ITO/n-WO_3 system, the band bending in the n-Si is a result of the Schottky barrier formed between the Si and the ITO. (d) When illuminated, a photovoltage is generated in the WO_3 ($V_{ph,1}$), as in the case of configuration (b). An additional photovoltage is generated because photons with energy smaller than the energy of the WO_3 band gap are absorbed in the Si, generating a second photovoltage ($V_{ph,2}$) at the solid-state junction. This additional photovoltage appears as a negative shift to the onset potential for photocurrent for the n-Si/ITO substrate relative to the behavior of the p-Si/ITO system (Figure 7c).

absorption in the Si substrate. Some of this absorption generates photocarriers in the space-charge region of the n-Si/ITO junction and thus generates a useful photovoltage. In principle, if this configuration generated sufficient photovoltage to split water, then this design could be translated directly into a device by the addition of an electrocatalyst directly to the back side of the Si wafer, to perform the H_2-evolution reaction. Conversely, a device designed to produce a photovoltage at a semiconductor–liquid junction on the back side of a planar Si electrode might not be as efficient if the material properties prevent photogenerated electrons and holes from reaching the space-charge region. However, a dual-semiconductor–liquid junction device is not limited in this way when light can reach the space-charge region of the photocathode. For example, a structured material geometry, such as semiconductor nanowires, could be used beneficially because such a device is mostly transparent and because light can be usefully absorbed at the photocathode on the back side of the sample.

V. CONCLUSIONS

The properties of the Si/n-WO_3 interface were in general accord with the band-edge alignment predicted by Andersen theory. p-Si provided an ohmic contact to electrodeposited n-WO_3 films, whereas rectifying behavior was observed for n-WO_3 films that were electrodeposited on n-Si substrates. The photocurrent of the Si/n-WO_3 system was limited by the properties of the interface rather than by the properties of the n-WO_3 or Si. XPS depth profiling indicated that no discernible insulating oxide layer was formed during deposition that would account for the current limitation. When a thin contacting layer of ITO was sputtered on the Si prior to electrodeposition of films of WO_3, the photoanodic performance of an identically prepared WO_3 film met or exceeded that for WO_3 on FTO. On n-Si substrates, a Schottky barrier was generated at the Si/ITO interface, and this junction contributed additional photovoltage to the monolithic n-Si/ITO/n-WO_3 photoanode structure. The ability to move the physical position of the photovoltage-generating junctions provides added flexibility in device design and is particularly helpful in cases where strategies for light trapping and structured materials can be utilized beneficially to improve the overall tandem device performance.

■ ASSOCIATED CONTENT

Supporting Information

Extra structural characterization and cyclic voltammetry measurements. This material is available free of charge via the Internet at http://pubs.acs.org.

■ AUTHOR INFORMATION

Corresponding Author

*Phone 626-395-6335; e-mail nslewis@caltech.edu.

Notes

The authors declare no competing financial interest.

■ ACKNOWLEDGMENTS

We acknowledge the Defense Advanced Research Projects Agency (DARPA) Grant W911NF-09-2-0011 for support of R.H.C. and N.S.L. and the Joint Center for Artificial Photosynthesis, a DOE Energy Innovation Hub, supported through the Office of Science of the U.S. Department of Energy under Award DE-SC0004993, for support of M.S., B.S.B., and N.S.L. We also acknowledge BP and the Molecular Materials Research Center of the Beckman Institute at the California Institute of Technology for support.

■ REFERENCES

(1) Gratzel, M. Photoelectrochemical Cells. *Nature* **2001**, *414*, 338–344.
(2) Dominey, R. N.; Lewis, N. S.; Bruce, J. A.; Bookbinder, D. C.; Wrighton, M. S. Improvement of Photoelectrochemical Hydrogen Generation by Surface Modification of p-Type Silicon Semiconductor Photocathodes. *J. Am. Chem. Soc.* **1982**, *104*, 467–482.
(3) Lehmann, V. *Electrochemistry of Silicon: Instrumentation, Science, Materials and Applications*; Wiley-VCH: Verlag GmbH, 2002.

(4) Hwang, Y. J.; Boukai, A.; Yang, P. High Density n-Si/n-TiO_2 Core/Shell Nanowire Arrays with Enhanced Photoactivity. *Nano Lett.* **2008**, *9*, 410−415.
(5) Mayer, M. T.; Du, C.; Wang, D. Hematite/Si Nanowire Dual-Absorber System for Photoelectrochemical Water Splitting at Low Applied Potentials. *J. Am. Chem. Soc.* **2012**, *134*, 12406−12409.
(6) Miller, E. L.; Paluselli, D.; Marsen, B.; Rocheleau, R. E. Development of Reactively Sputtered Metal Oxide Films for Hydrogen-Producing Hybrid Multijunction Photoelectrodes. *Sol. Energy Mater. Sol. Cells* **2005**, *88*, 131−144.
(7) Xu, Y.; Schoonen, M. A. A. The Absolute Energy Positions of Conduction and Valence Bands of Selected Semiconducting Minerals. *Am. Mineral.* **2000**, *85*, 543−556.
(8) Grimes, C.; Varghese, O.; Ranjan, S. *Light, Water, Hydrogen: The Solar Generation of Hydrogen by Water Photoelectrolysis*; Springer: Berlin, 2007.
(9) Meulenkamp, E. A. Mechanism of WO_3 Electrodeposition from Peroxy-Tungstate Solution. *J. Electrochem. Soc.* **1997**, *144*, 1664−1671.
(10) Mi, Q.; Zhanaidarova, A.; Brunschwig, B. S.; Gray, H. B.; Lewis, N. S. A Quantitative Assessment of the Competition between Water and Anion Oxidation at WO_3 Photoanodes in Acidic Aqueous Electrolytes. *Energy Environ. Sci.* **2012**.
(11) Gissler, W.; Memming, R. Photoelectrochemical Processes at Semiconducting WO_3 Layers. *J. Electrochem. Soc.* **1977**, *124*, 1710−1714.
(12) Ahlgren, W. L. Analysis of the Current-Voltage Characteristics of Photoelectrolysis Cells. *J. Electrochem. Soc.* **1981**, *128*, 2123−2128.
(13) Santato, C.; Ulmann, M.; Augustynski, J. Photoelectrochemical Properties of Nanostructured Tungsten Trioxide Films. *J. Phys. Chem. B* **2001**, *105*, 936−940.
(14) Yoon, K. H.; Shin, C. W.; Kang, D. H. Photoelectrochemical Conversion in a WO_3 Coated P-Si Photoelectrode: Effect of Annealing Temperature. *J. Appl. Phys.* **1997**, *81*, 7024−7029.
(15) Ashok, S.; Fonash, S. J.; Singh, R.; Wiley, P. On Resolving the Anomaly of Indium-Tin Oxide Silicon Junctions. *IEEE Electron Device Lett.* **1981**, *EDL-2*, 184−186.
(16) Anderson, R. L. Experiments on Ge-GaAs Heterojunctions. *Solid-State Electron.* **1962**, *5*, 341−351.
(17) Franciosi, A.; Van de Walle, C. G. Heterojunction Band Offset Engineering. *Surf. Sci. Rep.* **1996**, *25*, 1−140.
(18) Wang, W.; Chen, S.; Yang, P.-X.; Duan, C.-G.; Wang, L.-W. Si:WO_3 Heterostructure for Z-Scheme Water Splitting: An Ab Initio Study. *J. Mater. Chem. A* **2013**, *1*, 1078−1085.
(19) Khaselev, O.; Turner, J. A. A Monolithic Photovoltaic-Photoelectrochemical Device for Hydrogen Production Via Water Splitting. *Science* **1998**, *280*, 425−427.
(20) Miller, E. L.; Marsen, B.; Paluselli, D.; Rocheleau, R. Optimization of Hybrid Photoelectrodes for Solar Water-Splitting. *Electrochem. Solid-State Lett.* **2005**, *8*, A247.
(21) Alexander, B. D.; Kulesza, P. J.; Rutkowska, I.; Solarska, R.; Augustynski, J. Metal Oxide Photoanodes for Solar Hydrogen Production. *J. Mater. Chem.* **2008**, *18*, 2298−2303.
(22) Meng, L.; Dos Santos, M. Properties of Indium Tin Oxide (ITO) Films Prepared by RF-Reactive Magnetron Sputtering at Different Pressures. *Thin Solid Films* **1997**, *303*, 151−155.
(23) Tanisaki, S. Crystal Structure of Monoclinic Tungsten Trioxide at Room Temperature. *J. Phys. Soc. Jpn.* **1960**, *15*, 573−581.